

ORIGINAL ARTICLE

Dysregulated choline metabolism in T-cell lymphoma: role of choline kinase- α and therapeutic targetingJ Xiong^{1,6}, J Bian^{2,6}, L Wang^{1,3}, J-Y Zhou², Y Wang², Y Zhao^{1,3}, L-L Wu⁴, J-J Hu⁵, B Li⁵, S-J Chen^{1,3}, C Yan² and W-L Zhao^{1,3}

Cancer cells have distinct metabolomic profile. Metabolic enzymes regulate key oncogenic signaling pathways and have an essential role on tumor progression. Here, serum metabolomic analysis was performed in 45 patients with T-cell lymphoma (TCL) and 50 healthy volunteers. The results showed that dysregulation of choline metabolism occurred in TCL and was related to tumor cell overexpression of choline kinase- α (Choka). In T-lymphoma cells, pharmacological and molecular silencing of Choka significantly decreased Ras-GTP activity, AKT and ERK phosphorylation and MYC oncoprotein expression, leading to restoration of choline metabolites and induction of tumor cell apoptosis/necroptosis. In a T-lymphoma xenograft murine model, Choka inhibitor CK37 remarkably retarded tumor growth, suppressed Ras-AKT/ERK signaling, increased lysophosphatidylcholine levels and induced *in situ* cell apoptosis/necroptosis. Collectively, as a regulatory gene of aberrant choline metabolism, Choka possessed oncogenic activity and could be a potential therapeutic target in TCL, as well as other hematological malignancies with interrupted Ras signaling pathways.

Blood Cancer Journal (2015) 5, 287; doi:10.1038/bcj.2015.10; published online 13 March 2015

INTRODUCTION

T-cell lymphoma (TCL) is the malignant proliferation of CD3+ lymphocytes and represents one of the main subtypes of non-Hodgkin's lymphoma.^{1,2} TCL patients are generally resistant to conventional chemotherapy and have poor clinical outcome. Varied with pathological, immunophenotypic and molecular features, TCL constitutes a heterogeneous group of diseases.^{3,4} Therefore, biomarkers commonly expressed and closely related to tumor progression need to be further investigated in TCL, helping to develop targeted therapeutic approaches and to eventually improve prognosis of the patients.

In addition to genomic, epigenomic and proteomic alterations, perturbation of cellular metabolism occurs in cancers and contributes fundamentally to tumorigenicity.⁵ Dysregulated choline metabolism has recently emerged as an important metabolic hallmark of cancer cells. The biosynthesis of phosphocholine mediates mitogenic activity and is required for uncontrolled tumor cell growth.⁶ Moreover, choline metabolism could interact with multiple oncogenic cascades, facilitating tumor progression.⁷ However, the metabolomic profile, particularly choline metabolism and its relation with cellular signaling pathways have not yet been illustrated in TCL.

Choline kinase- α (Choka), a family member of initial enzyme involved in the regulation of choline metabolism, leads to the phosphorylation of choline to phosphocholine.⁷ Choka is frequently overexpressed in cancers and associated with adverse disease outcome and high histological grade.^{8,9} Here, we assessed the metabolic phenotype of the TCL patients, as well as the molecular mechanism and the interconnected network underlying

this phenotype. Our results provided direct evidence that aberrant choline metabolism occurred in TCL, relating to the upregulation of Choka and downstream activation of Ras-AKT/ERK-MYC signaling pathway. Both *in vitro* and *in vivo*, therapeutic inhibition of Choka displayed significant antiproliferative effect by inducing tumor cell apoptosis and necroptosis, making Choka an attractive molecular target for treating TCL, as well as other Ras-activated hematological malignancies.

MATERIALS AND METHODS

Patients

A metabolomic assay was performed on serum samples of 45 patients with TCL (including 16 peripheral TCL, not other specified, 11 natural killer/TCL, 6 cutaneous TCL), 6 T-lymphoblastic lymphoma, 3 anaplastic large-cell lymphoma and 3 angioimmunoblastic TCL (AITL). Quantitative reverse transcription-PCR was performed on frozen tumor samples of 81 TCL cases (including 28 peripheral TCL, not other specified, 16 natural killer/TCL, 4 cutaneous TCL, 11 T-lymphoblastic lymphoma, 8 anaplastic large-cell lymphoma and 14 AITL). Histological diagnoses were established according to the World Health Organization classification.¹⁰ Fifty age- and sex-matched healthy volunteers and 33 cases of reactive hyperplasia were referred as controls. Informed consent was obtained from all the patients and volunteers in accordance with the Declaration of Helsinki. The study was approved by the Hospital Review Board.

Metabolomic assay by UPLC-QTOFMS

Serum sample (100 μ l) was added by 50 μ l L-2-chlorophenylalanine (0.2 mg/ml), vortexed for 30 s and then mixed with 350 μ l organic solvents (methanol/acetonitrile, 2/1). After incubation for 15 min at 4 °C,

¹State Key Laboratory of Medical Genomics, Shanghai Institute of Hematology, Shanghai Rui Jin Hospital, Shanghai Jiao Tong University School of Medicine, Shanghai, China;

²School of Pharmacy, Shanghai Jiao Tong University, Shanghai, China; ³Pôle de Recherches Sino-Français en Science du Vivant et Génomique, Laboratory of Molecular Pathology, Shanghai, China;

⁴Department of Pathology, Shanghai Rui Jin Hospital, Shanghai Jiao Tong University School of Medicine, Shanghai, China and ⁵Department of Nuclear Medicine, Shanghai Rui Jin Hospital, Shanghai Jiao Tong University School of Medicine, Shanghai, China. Correspondence: Professor C Yan, School of Pharmacy, Shanghai Jiao Tong University, 800 Dongchuan Road, Shanghai 200240, China or Professor W-L Zhao, State Key Laboratory of Medical Genomics, Shanghai Institute of Hematology, Shanghai Rui Jin Hospital, Shanghai Jiao Tong University School of Medicine, 197 Rui Jin Er Road, Shanghai 200025, China.

E-mail: chaoyan@unimicrotech.com or zhao.weili@yahoo.com

⁶These authors contributed equally to this work.

Received 10 July 2014; revised 12 December 2014; accepted 13 January 2015

the mixture was centrifuged at 15 000 r.p.m. for 15 min and 200 μ l supernatant was used for ultra-performance liquid chromatography quadrupole time-of-flight mass spectrometry (UPLC-QTOFMS) analysis. The in-house quality control sample was prepared by pooling the same volume of serum samples from healthy volunteers, as reported previously.¹¹

Reversed-phase separation was performed on a 2.1 \times 100 mm² ACQUITY 1.7 μ m BEH C18 column (Waters Corp., Milford, MA, USA) according to the manufacturer's instruction. The mobile phase consisted of (A) water with 0.1% formic acid and (B) acetonitrile with 0.1% formic acid. MS was performed on Waters Q-TOF Micromass (Waters Corp.) in both positive and negative ion modes at a resolution of 8000. The detailed conditions of mobile phase and parameters of MS analysis were provided in Supplementary Experimental procedures.

Analysis of metabolites by UPLC-3QMS

Metabolites of cells (1×10^7 /ml) were extracted using freeze-thaw method.¹² Cell lysate (100 μ l) was mixed with 100 μ l organic solvents (methanol/acetonitrile, 1/1). After incubation for 15 min at 4 °C, the mixture was centrifuged at 15 000 r.p.m. for 15 min and 150 μ l supernatant was used for ultra-performance liquid chromatography-triple quadrupole MS (UPLC-3QMS) analysis.

The quantitative analysis using multiple reaction monitoring approach was performed on a 2.1 \times 50 mm² ACQUITYTM 1.7 μ m BEH C18 column (Waters Corp.) for lipid metabolites, a 2.1 \times 50 mm² ACQUITYTM 1.7 μ m BEH HILIC column (Waters Corp.) for choline and SCIEX SelexION Triple Quad S5500 System mass spectrometer (AB Corp., Short Hills, NJ, USA) in positive and negative ion modes, respectively. The detailed parameters were provided in Supplementary Experimental procedures.

Quantitative real-time PCR

Total mRNA was extracted from frozen tumor samples using TRIzol reagent (Invitrogen, Shanghai, China) and complementary DNA was synthesized from 100 ng RNA using PrimeScript RT Reagent Kit with gDNA Eraser (TaKaRa, Dalian, China). Quantitative real-time PCR was performed using SYBR Premix Ex TaqTM II (TaKaRa) and ABI Prism 7500 (Applied Biosystems, Bedford, MA, USA) with primers against *SLC44A1*, *CHKA*, *PCYT1A*, *PLD2*, *PLCG2*, *PLA1A* and *PLA2G4A*. *GAPDH* was used as an endogenous control. Primer sequences are listed in Supplementary Experimental procedures.

Cell lines and reagents

T-lymphoma cell lines Jurkat and H9 (American Type Culture Collection, Manassas, VA, USA) were cultured in RPMI-1640 medium supplemented with 10% heat-inactivated fetal bovine serum in a humidified atmosphere of 95% air and 5% CO₂ at 37 °C. Choka inhibitor (CK37), phosphatidylinositol 3-kinase (PI3K) inhibitor (LY294002) and ERK inhibitor (FR180204) were obtained from Merck KGaA (Darmstadt, Germany). Pancaspase inhibitor (Z-VAD-FMK) was from APEXBIO (Houston, TX, USA).

Cell viability and cell apoptosis

Cell growth was assessed by MTT (3-(4,5-dimethylthiazol-2-yl)-2,5-diphenyltetrazolium bromide) and absorbance was measured at 490 nm by spectrophotometry. Cell apoptosis were detected by flow cytometry (BD, Biosciences, San Jose, CA, USA) using Annexin V-FITC Apoptosis Kit (BD, Pharmingen, San Diego, CA, USA).

Small-interfering RNA transfection

Cells were transfected with 50 nm Choka siGENOME SMARTpool and Non-Targetingpool (Dharmacon, Denver, CO, USA) as a negative control using DharmaFECT2 transfection reagents (Dharmacon).

Ras activation assay

Ras activity was assessed by Ras Pull-down Activation Assay Biochem Kit (bead pull-down format) (Cytoskeleton, Denver, CO, USA) according to the manufacturer's protocol.

Western blot

Western blot was performed as described previously.¹⁰ Antibodies against Choka, c-MYC and ERK were obtained from Abcam (Cambridge, UK).

Antibodies against Ras, phosphorylation of AKT (p-AKT) (Ser473), AKT, phosphorylation of ERK (p-ERK) (Thr202/Tyr204) and RIP3 were from Cell Signaling (Beverly, MA, USA). Actin (Cell Signaling) was used to ensure equivalent loading of total protein.

Co-immunoprecipitation assay

Co-immunoprecipitation assay was performed by Pierce Co-Immuno-precipitation Kit (Thermo, Pierce, Rockford, IL, USA) according to the manufacturer's protocol. Cell lysate was immunoprecipitated with resins coupled with anti-human RIP1 (BD Pharmingen, San Diego, CA, USA) overnight at 4 °C.

Human TNF- α immunoassay

Tumor necrosis factor- α (TNF- α) was measured using Human TNF- α Quantikine ELISA Kit (R&D Systems, Minneapolis, MN, USA) according to the manufacturer's protocol.

Immunohistochemistry and immunofluorescence assay

Immunohistochemistry was performed on 5- μ m paraffin sections with an indirect immunoperoxidase method using antibodies against Choka (Santa Cruz Biotechnology, Dallas, TX, USA), p-AKT, p-ERK (Cell Signaling) and MYC (Abcam). Immunofluorescence assay was performed on acetone-fixed cells using rabbit anti-human MYC as a primary antibody and diamino-triazinylaminofluorescein-labeled donkey anti-rabbit-IgG antibody (Abcam) as a secondary antibody. Nuclei were counterstained with DAPI (4',6'-diamidino-2-phenylindole).

Transmission electron microscopy

Cells and tissue samples were fixed for 2 h in 2% glutaraldehyde/0.1 M phosphate-buffered saline (pH 7.3) at 4 °C, rinsed with 0.1 M phosphate-buffered saline two times for 10 min at 4 °C, postfixed in 1% osmium tetroxide/0.1 M phosphate-buffered saline for 2 h at 4 °C, dehydrated in graded ethanol, saturated in graded Epikote and embedded. Ultrathin sections were prepared with LKB V ultramicrotome (LKB, Bromma, Sweden), stained with lead citrate and finally viewed with Philip CM-120 transmission electron microscope (Philips, Eindhoven, The Netherlands).

Gene network and pathway analysis

Human Genome U133 Plus 2.0 Array GeneChip microarray (Affymetrix, Santa Clara, CA, USA) was performed on frozen tumor samples of 8 TCL patients. Genes were subsequently filtered by comparing their expression levels according to Chok- α (*CHKA*) expression. Statistical differences were calculated and genes with $P < 0.05$ were analyzed for enrichment of KEGG (Kyoto Encyclopedia of Genes and Genomes) pathways. Genes significantly involved in the pathways were hierarchical clustered using MEV v.4.8.1 (Dana-Farber Cancer Institute, Boston, MA, USA).

Murine model

Nude mice (5–6 weeks old; Shanghai Laboratory Animal Center, Shanghai, China) were injected subcutaneously with 4×10^7 Jurkat cells into the flank. Treatments (10 mice per group) were started after tumor become about 0.5×0.5 cm² in surface (day 0). The untreated group received vehicle dimethyl sulfoxide, whereas the treated group received CK37 (4 mg/kg per day) once daily for 8 days. Tumor volume was calculated as $0.5 \times a$ (length) $\times b$ (width)². Animals were used according to the protocols approved by the Shanghai Rui Jin Hospital Animal Care and Use Committee.

Micro-PET/CT imaging

Mice were subjected to positron emission tomography-computed tomography (PET/CT) analysis after 1 week of treatment. PET/CT imaging was performed on an Inveon MM Platform (Siemens Preclinical Solutions, Knoxville, TN, USA) with 8.5 cm transaxial and 5.7 cm axial fields of view. ¹⁸F-fluorodeoxyglucose (0.1 ml per injection with an activity of 10 MBq) was injected to anesthetized mice through the tail vein. Mice were placed prone on the PET scanner bed 45 min later near the central field of view for scanning process in Inveon Acquisition Workplace 1.5.0.28. Ten-minute CT X-ray for attenuation correction was scanned with a power of 80 kV and 500 μ A and an exposure time of 1100 ms before PET scan.

Ten-minute static PET scans were then acquired, and images were reconstructed by an OSEM3D (three-dimensional ordered subsets expectation maximum) algorithm followed by MAP (maximization/maximum a posteriori) or FastMAP provided by Inveon Acquisition Workplace. The three-dimensional regions of interest were drawn over the heart guided by CT images and tracer uptake was measured using the software of Inveon Research Workplace (IRW) 3.0. Individual quantification of the ^{18}F -fluorodeoxyglucose uptake in each of them was calculated. Mean standardized uptake values were determined by dividing the relevant regions of interest concentration by the ratio of the injected activity to the body weight.

Statistical analysis

The UPLC-QTOFMS ESI+ and ESI- data were analyzed by the MarkerLynx Applications Manager version 4.1 (Waters Corp.). Multivariate analysis was performed using SIMCA-P software version 12.0 (Umetrics AB, Umeå, Sweden). The combinative effects were determined by the computer software CalcuSyn (Biosoft, Cambridge, UK). Variance between different groups was determined by two-tailed Student's *t*-test or Mann-Whitney *U*-test. Association between different factors or parameters was determined by χ^2 test. *P* < 0.05 was considered significant. Values were presented as mean \pm s.e.m. (*N* = 3 unless otherwise noted in the Figure legends). Statistical analyses were performed on SPSS 13.0 software (IBM Corp., Armonk, NY, USA).

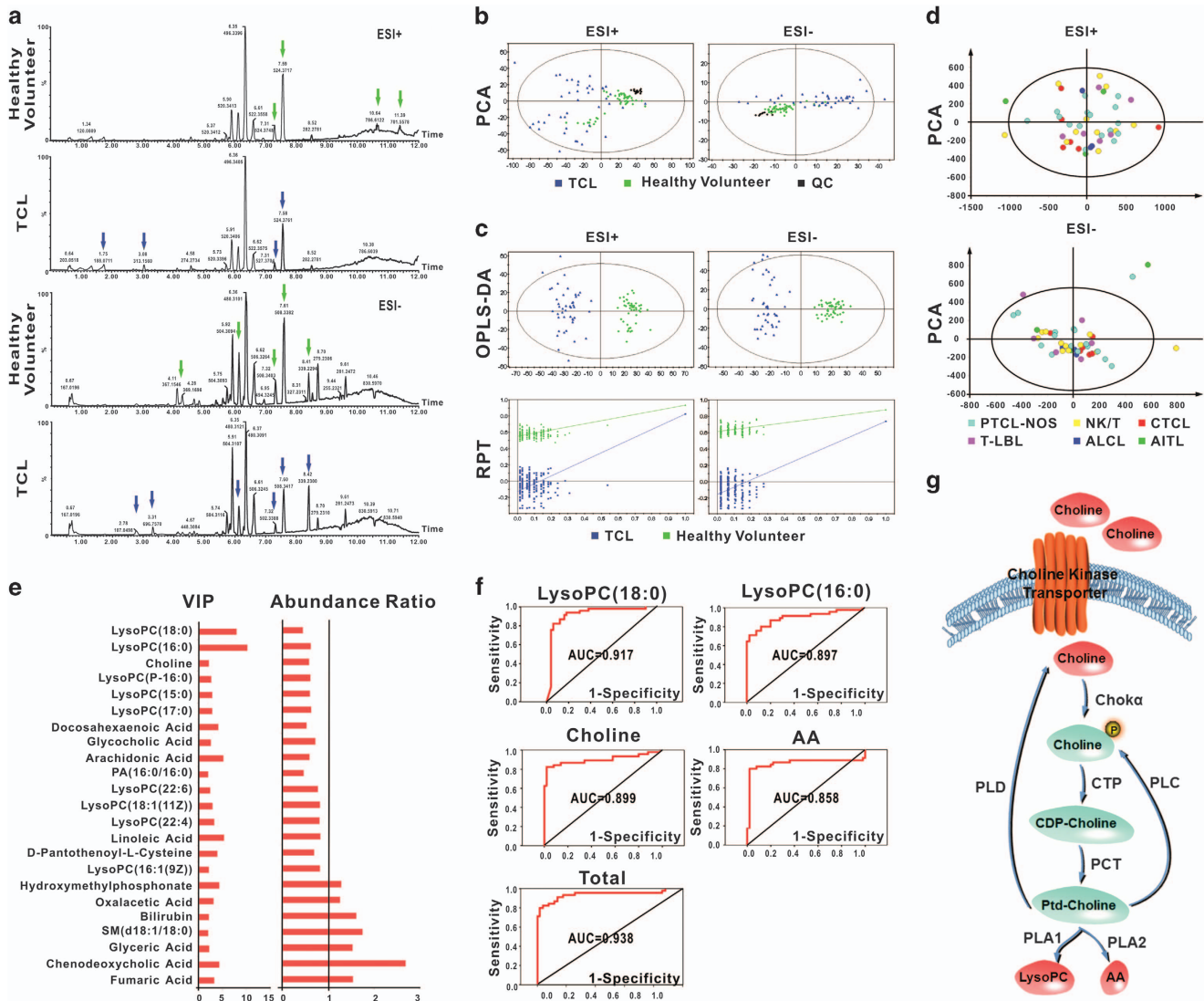


Figure 1. Metabolic profile indicated aberrant choline metabolism in patients with TCL. (a) Representative base peak intensity chromatograms of the TCL patients and the healthy volunteers detected by UPLC-QTOFMS under ESI+ and ESI- mode. Different peaks were marked by arrows. (b) The score plots of the principal component analysis (PCA) model was set up using data from 45 TCL patients (blue plots), 50 healthy volunteers (green plots) and 17 repeated quality controls (QCs, black plots). (c) The score plots of the orthogonal partial least-squared discrimination analysis (OPLS-DA) models (upper panels) discriminated the TCL group (blue plots) from the healthy volunteers (green plots), and was confirmed by response permutation test (RPT, lower panels). (d) The score plots of the PCA models according to histological subtypes of TCL (peripheral TCL, not other specified (PTCL-NOS), *N* = 16, light blue plots, natural killer/TCL (NK/T) lymphoma, *N* = 11, yellow plots, cutaneous TCL (CTCL), *N* = 6, red plots, T-lymphoblastic lymphoma (T-LBL), *N* = 6, purple plots, anaplastic large-cell lymphoma (ALCL), *N* = 3, dark blue plots, AITL, *N* = 3, green plots). (e) Metabolites with variable importance in projection (VIP) > 2 were divided into two groups according to abundance ratio (TCLs/healthy volunteers): upregulation (abundance ratio > 1) and downregulation (abundance ratio < 1). (f) Receiver operating characteristic (ROC) curve for LysoPC (18:0), LysoPC (16:0), choline, arachidonic acid (AA) and total between TCL patients and healthy volunteers. The sensitivity and specificity were 0.828 and 0.936 for LysoPC (18:0), 0.714 and 0.975 for LysoPC (16:0), 0.812 and 0.975 for choline, 0.797 and 0.974 for AA and 0.822 and 0.960 for Total, respectively. (g) Schematic description of choline metabolism. CTP, phosphocholine cytidyltransferase; PCT, diacylglycerol choline phosphotransferase; PLD, phospholipase D; PLC, phospholipase C; and PLA, phospholipase A.

RESULTS

Serum metabolomic profile revealed dysregulation of choline metabolism in patients with TCL

Serum metabolomic profile was assessed by UPLC-QTOFMS ESI+ and ESI- in 45 patients with TCL and 50 healthy volunteers as the normal control. The clinical characteristics of the patients were listed in Supplementary Table S1. As shown in Figure 1a, chromatogram of base peak intensity in TCL cases apparently differed from that of healthy controls. Principal component analysis score plots were analyzed on 1306 features obtained after normalization, including 778 spectral features for UPLC-QTOFMS ESI+ and 528 spectral features for UPLC-QTOFMS ESI-. The results showed the separation trend among the TCL patients, healthy volunteers and the repeated quality controls (Figure 1b). Subsequently, two cross-validated orthogonal partial least-squares discrimination analysis models were established and revealed satisfactory modeling and predictive abilities with one predictive component and three orthogonal components ($R^2X=0.449$, $R^2Y=0.915$, and $Q^2Y=0.708$) for UPLC-QTOFMS ESI+, one predictive component and two orthogonal components ($R^2X=0.236$, $R^2Y=0.895$ and $Q^2Y=0.737$) for UPLC-QTOFMS ESI-, respectively (Figure 1c (upper panel) and Supplementary Table S2), indicating the distinct serum metabolomic profile of TCL patients. A response permutation test with 200 random permutations was then performed in the partial least-squares discriminant analysis models and R^2 and Q^2 values derived from the permuted analysis

were all significantly lower than corresponding original values ($R^2Y=0.915$ and $Q^2Y=0.708$ for ESI+, $R^2Y=0.895$ and $Q^2Y=0.737$ for ESI-; Figure 1c (lower panel) and Supplementary Table S2), which validated the fitness of data and the predictive ability of the metabolomic method.

According to histological types of TCL, principal component analysis score plots showed similar distribution among the subgroups (Figure 1d). As for orthogonal partial least-squared discrimination analysis models, most of the Q^2 values of UPLC-QTOFMS ESI+ were < 0.5 , whereas those of UPLC-QTOFMS ESI- in natural killer/TCL vs AITL, cutaneous TCL vs AITL and anaplastic large-cell lymphoma vs AITL were 0.693, 0.641 and 1, respectively (Supplementary Table S3). However, R^2 and Q^2 values of response permutation test were higher than or equal to corresponding original values in these subgroups, suggesting that the metabolomic profile was similar in all these histological types studied (Supplementary Figure S1A).

Significantly altered serum metabolites with the variable importance in projection threshold > 2 in the above-mentioned orthogonal partial least-squared discrimination analysis models and selected by the Mann-Whitney U -test ($P < 0.05$) were identified in patients with TCL and listed in Figure 1e, including 16 metabolites lower (abundance ratio < 1) and 7 higher (abundance ratio > 1) than healthy volunteers. Interestingly, 17 of these 23 metabolites were related to lipid metabolism. Among them, lysophosphatidylcholine (LysoPC) (18:0), LysoPC (16:0), choline and arachidonic acid (AA) presented relatively higher

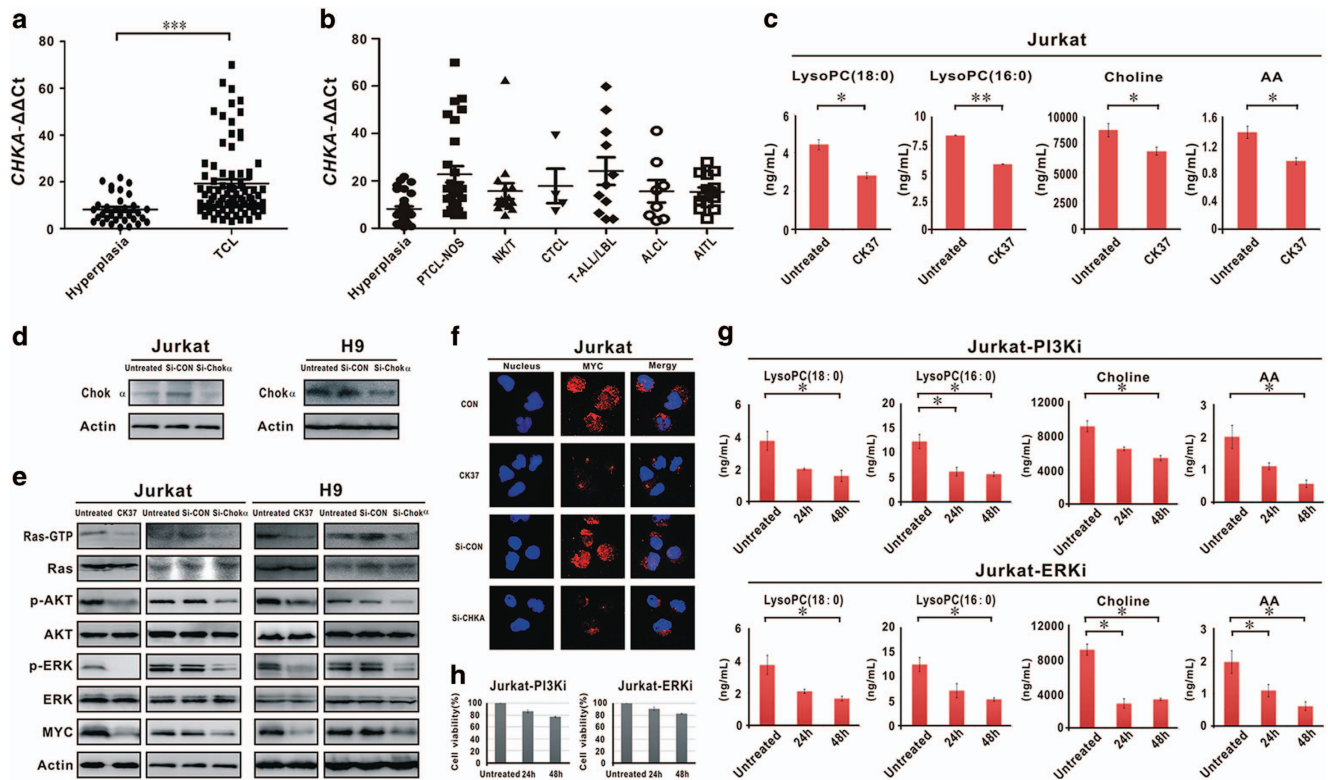


Figure 2. Chok α was overexpressed in TCL patients and related to dysregulation of choline metabolism through activating Ras-AKT/ERK-MYC axis. (a) Comparing with reactive hyperplasia, CHKA was overexpressed in TCL patients ($***P < 0.001$). (b) Comparing with reactive hyperplasia, elevated CHKA levels were observed among all the subtypes studied. (c) Treatment with Chok α inhibitor CK37 (3 μ M) in Jurkat cells decreased expression of LysoPC (18:0), LysoPC (16:0), choline and AA. $***P < 0.01$, $*P < 0.05$ compared with the untreated group. (d) The extent of Chok α knockdown by small-interfering RNA in both Jurkat and H9 cells were shown by western blot. (e) In Jurkat and H9 cells, pharmacological silencing of Chok α by CK37 and molecular inhibition of Chok α by siRNA (Si-Chok α) significantly reduced the activity of Ras-GTP, as well as protein levels of p-AKT, p-ERK and MYC. Si-CON, cells transfected with non-targeting siRNA. (f) MYC expression downregulated when transfected with Chok α siRNA or treated with CK37 was further validated by immunofluorescence assay. (g and h) Twenty-four or 48 h treatment with PI3K inhibitor LY294002 (PI3Ki) (25 μ M) or ERK inhibitor FR180204 (ERKi) (30 μ M) in Jurkat cells significantly decreased the expression of LysoPC (18:0), LysoPC (16:0), choline and AA (g), without affecting cell viability (h). $*P < 0.05$ compared with the untreated group. Data in (a), (b), (c), (g) and (h) were represented as mean \pm s.e.m.

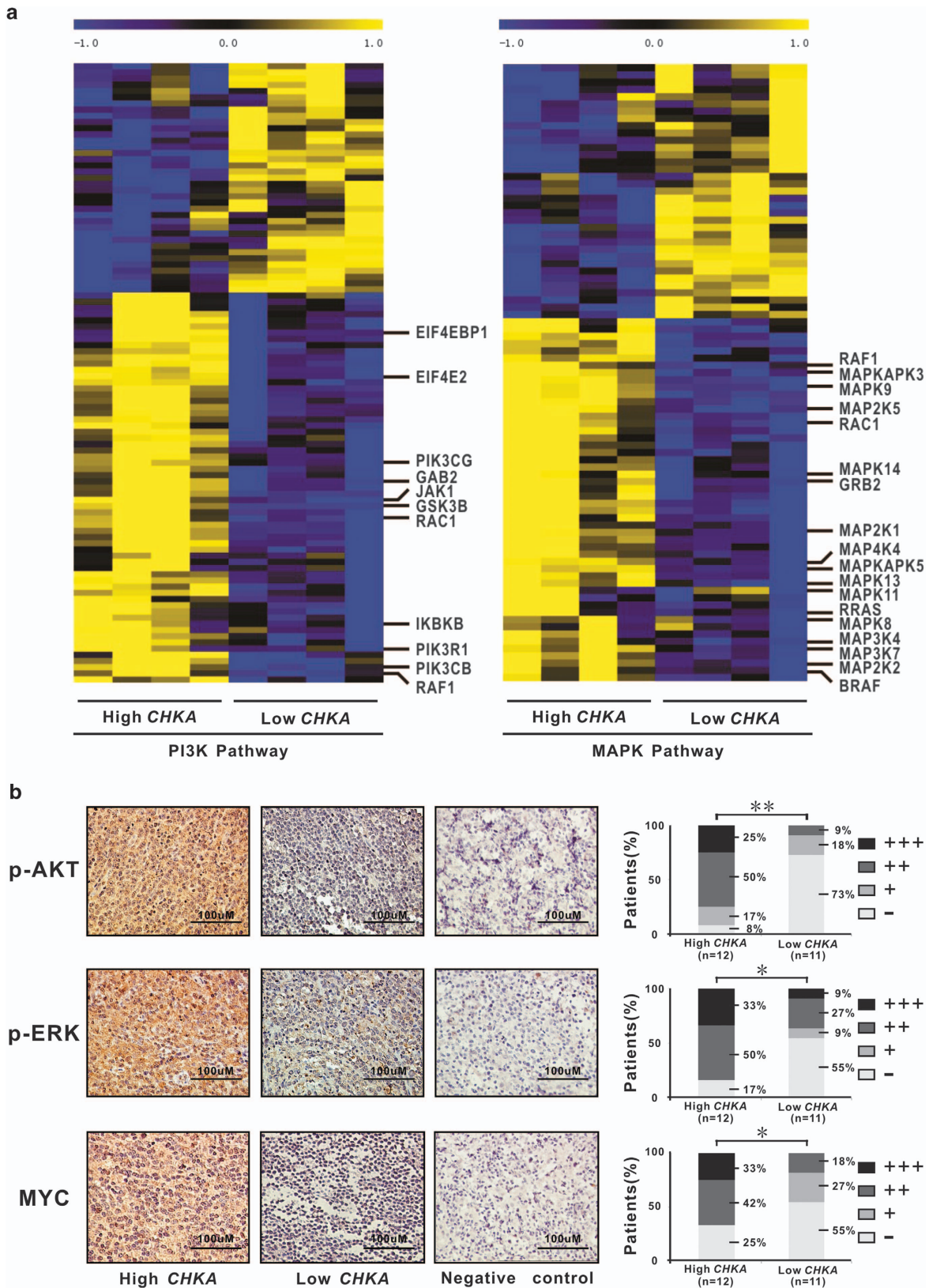


Figure 3. PI3K and MAPK pathway expression in patients with TCL. **(a)** Gene sets of PI3K and MAPK pathway were analyzed by gene network and pathway analysis on microarray data of TCL according to *CHKA* expression. The key genes in PI3K and MAPK pathway were indicated on the right side of the heat maps. **(b)** As revealed by immunohistochemistry, increased positivity of p-AKT, p-ERK and MYC expression were observed in tumor samples of TCL patients with high *CHKA* expression. The tissue samples of reactive hyperplasia were referred as a negative control. $**P < 0.01$, $*P < 0.05$ compared with those with low *CHKA* expression. Data in **(b)** were represented as mean \pm s.e.m.

variable importance in projection value and were all significantly decreased in the TCL group. Validated by the receiver operating characteristic analysis (Figure 1f), the area under curve values of the four metabolites were 0.917, 0.897, 0.899 and 0.858, respectively, with the total area under curve value as 0.938, confirming the efficiency of these metabolic markers in differentiating between TCL cases and healthy controls. Therefore, choline metabolism was dysregulated in TCL, as schematically summarized in Figure 1g.

Choka was overexpressed in TCL and related to aberrant choline metabolism

The main regulatory enzymes of choline metabolism were measured by real-time quantitative PCR, namely Choka (*CHKA*), Chok transporter (*SLC44A*), phosphocholine Cytidyltransferase (*PCYT1A*), phospholipase D (*PLD2*), phospholipase C (*PLCG2*), phospholipase A1 (*PLA1A*) and phospholipase A2 (*PLA2G4A*). Comparing with reactive hyperplasia, *CHKA* was overexpressed in patients with TCL ($P < 0.001$; Figure 2a), without statistical variation in other regulatory enzymes (Supplementary Figure S1B). As shown in Figure 2b, upregulation of *CHKA* was found

irrespective of TCL subgroups, consistent with their similar metabolomic profile (Figure 1d).

To determine whether Choka was functionally relevant to choline metabolism, Jurkat cells were treated with CK37, a specific inhibitor of Choka. Assessed by (UPLC-3QMS), the levels of LysoPC (18:0), LysoPC (16:0), choline and AA were significantly reduced upon CK37 treatment (Figure 2c), confirming the biological role of Choka on regulating choline metabolites in T-lymphoma cells.

Choka modulated choline metabolism through Ras-AKT/ERK signaling pathway

To gain insight into the molecular mechanism of Choka in the regulation of choline metabolism in TCL, Choka was modulated in Jurkat and H9 cells by treatment with Choka inhibitor CK37 or transfection with specific small-interfering RNA (siRNA) targeting Choka (Si-Choka). Based on previous reports,^{13,14} we focused on Ras-AKT/ERK signaling pathway. Pharmacological and molecular silencing of Choka significantly reduced the activity of Ras-GTP, an active form of Ras protein (Figure 2d). Meanwhile, p-AKT and p-ERK were decreased in CK37-treated or Si-Choka-transfected lymphoma cells, whereas total AKT and ERK levels remained unchanged (Figure 2d). MYC has an important role in lymphoma

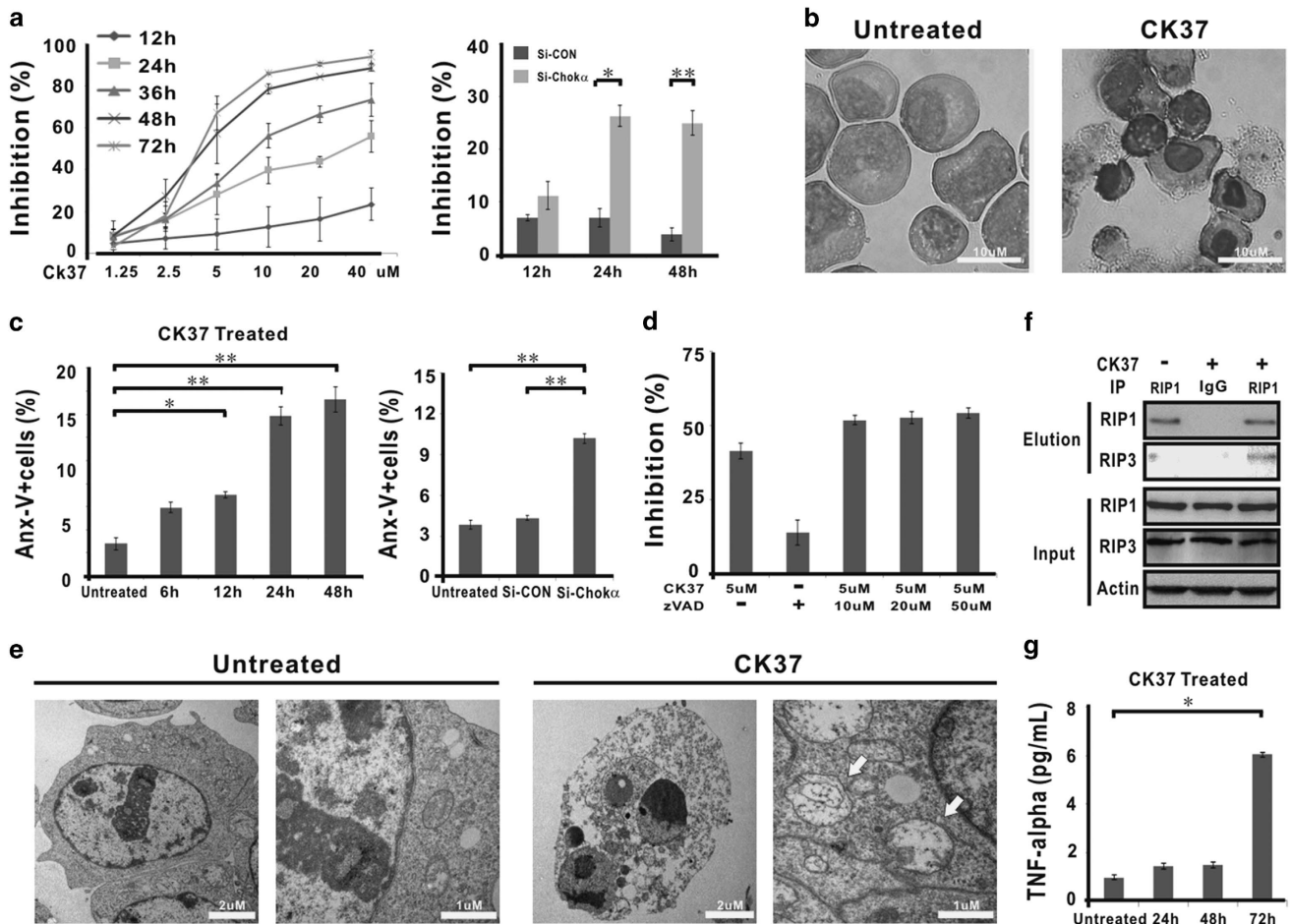


Figure 4. Therapeutic targeting of Chok α inhibited T-lymphoma cell proliferation and induced cell death via apoptosis and necroptosis. (a) CK37 inhibited Jurkat cell growth in a time- and dose-dependent manner (left panel). Growth inhibition was also observed in Jurkat cells transfected with Chok α siRNA (Si-Chok α ; right panel). $**P < 0.01$, $*P < 0.05$ compared with Si-CON. (b) Wright's staining showed characteristic apoptotic cells after CK37 (5 μ M) treatment. (c) Percentage of Annexin-V-positive cells significantly increased in CK37-treated and Si-Chok α -transfected cells. $**P < 0.01$, $*P < 0.05$ compared with the untreated group. (d) Pancaspase inhibitor Z-VAD-FMK only partially counteracted CK37-induced cell growth inhibition. (e) Transmission electron microscopy showed typical necroptotic cells after CK37 treatment. (f) Co-immunoprecipitation showed increased formation of RIP1-RIP3 complex in CK37-treated cells. (g) CK37 induced TNF- α secretion. $*P < 0.05$ compared with the untreated group. Data in (a), (c), (d) and (g) were represented as mean \pm s.e.m.

progression and is regulated by AKT and ERK in TCL.¹³ In Jurkat and H9 cells, the extent of Choka knockdown were validated by western blot (Figure 2d). In parallel with dephosphorylation of AKT and ERK, MYC expression was downregulated when treated with CK37 or Si-Choka, as revealed by western blot (Figure 2e) and immunofluorescence assay (Figure 2f). When Jurkat cells were treated with the PI3K inhibitor LY294002 or the ERK inhibitor FR180204, expressions of LysoPC (18:0), LysoPC (16:0), choline and AA were remarkably downregulated (Figure 2g), whereas cell viability remained > 80% (Figure 2h), indicating that Choka regulated choline metabolism in a PI3K- and mitogen-activated protein kinase (MAPK)-dependent manner. These results demonstrated that Choka regulated choline metabolism by targeting Ras, as well as downstream AKT, ERK and MYC expression.

Clinically, gene expression profile was analyzed in tissue samples of eight patients with TCL. Using KEGG database, altered genes were enriched in PI3K and MAPK pathways according to *CHKA* expression of the TCL cases (Figure 3a). Moreover, p-ERK, p-AKT and MYC expression were detected by immunohistochemistry in 23 TCL tumor sections, including 12 cases with high *CHKA* expression group (>median level of *CHKA* expression in TCL) and 11 cases with low *CHKA* expression group (< median level of *CHKA* expression in TCL). Upregulation of *CHKA* correlated with increased positivity of p-AKT ($P=0.008$), p-ERK ($P=0.029$) and MYC expression ($P=0.047$, Figure 3b). These data further confirmed that Choka was related to the activation of PI3K and MAPK signaling cascades, as well as MYC overexpression.

Therapeutic targeting of Choka inhibited T-lymphoma cell proliferation via inducing apoptosis and necroptosis

As shown in Figure 4a, CK37 exhibited a remarkable reduction in Jurkat cell growth in a time- and dose-dependent manner (left panel), which was also observed in Jurkat cells transfected with Si-Choka (right panel). CK37-treated cells displayed characteristic morphological changes of apoptosis, such as shrinking cytoplasm, condensed chromatin and nuclear fragmentation with intact cell membrane (Figure 4b). Accordingly, the percentage of Annexin-V+ cells was significantly increased in CK37-treated and Si-Choka-transfected cells (Figure 4c).

However, the addition of pancaspase inhibitor Z-VAD-FMK failed to rescue cell growth inhibition induced by CK37 (Figure 4d), raising the hypothesis that other biological effect could be involved in CK37-mediated lymphoma cell death. Besides apoptosis, necroptosis is another important modality of cell death.¹⁵ Indeed, under transmission electron microscopy, CK37-treated Jurkat cells presented loss of plasma membrane integrity, swelling mitochondria and intact nuclei membrane, which are typical morphological characteristics of necroptosis (Figure 4e). To verify that necroptosis occurred simultaneously with apoptosis upon CK37 treatment, co-immunoprecipitation was performed and showed increased binding activity between RIP1 and RIP3 (RIP1/RIP3 complex, also known as necrosome; Figure 4f). It has been recently reported that TNF- α is a main inducer of necroptosis.¹⁶ Detected by ELISA (enzyme-linked immunosorbant assay), TNF- α concentration of cell culture supernatant elevated gradually, reaching the peak at 72 h after CK37 treatment (Figure 4g), confirming that CK37 stimulated TNF- α synthesis and induced necroptosis in T-lymphoma cells.

Furthermore, the combined effect of CK37 with chemotherapeutic and biotherapeutic agents applied in lymphoma treatment was evaluated. Of note, combination index plots showed synergistic interactions of CK37 with second-line chemotherapeutic agents such as cisplatin and gemcitabine, but not first-line agents such as doxorubicin and cyclophosphamide.

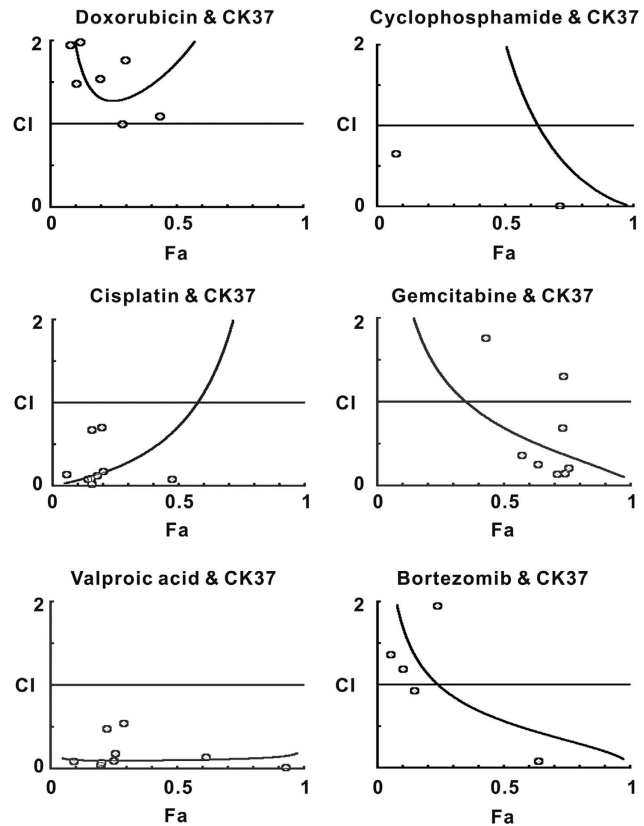


Figure 5. Therapeutic targeting of Choka synergized with chemotherapeutic and biotherapeutic agents. Combination index plots showed the data points under the curve (CI = 1), indicating that the combination was synergistic in Jurkat cells cotreated with CK37 and cisplatin, gemcitabine or valproic acid.

Synergism was also observed in cells cotreated with CK37 and histone deacetylase inhibitor valproic acid, but not with proteasome inhibitor bortezomib (Figure 5).

Therapeutic targeting of Choka suppressed tumor growth *in vivo* through the downregulation of Ras-AKT/ERK-MYC axis and induction of cell apoptosis/necroptosis

In the murine model established with subcutaneous injection of Jurkat cells, xenograft tumors formed at the site of injection in all mice. The sizes of tumors in the CK37 group were significantly smaller than those of the untreated group since 2 days of treatment (Figure 6a). ¹⁸F-fluorodeoxyglucose small-animal PET/CT was further performed to visualize tumors implanted in the flank of nude mice at 8 days of treatment (Figure 6b). Comparing with the healthy and the untreated mice, standardized uptake value intensity of the CK37-treated tumors was significantly decreased (Figure 6b). Accordingly, serum levels of LysoPC (18:0) and LysoPC (16:0) were also restored following treatment with CK37 (Figure 6c).

As *in vitro* study, compared with the untreated group, p-AKT, p-ERK and MYC expression were significantly decreased in the tumor of the CK37 group (Figure 6d), along with reduced activity of Ras-GTP (Figure 6e). To search for more evidence of tumor cell apoptosis and necroptosis, TUNEL (terminal deoxynucleotidyl transferase-mediated dUTP nick-end labeling assay) assay and ultrastructural study were also performed on mice tumor sections, respectively. The number of apoptotic tumor cells was significantly higher in the CK37 group than those in the untreated group ($P=0.008$; Figure 6f). Meanwhile, CK37-treated

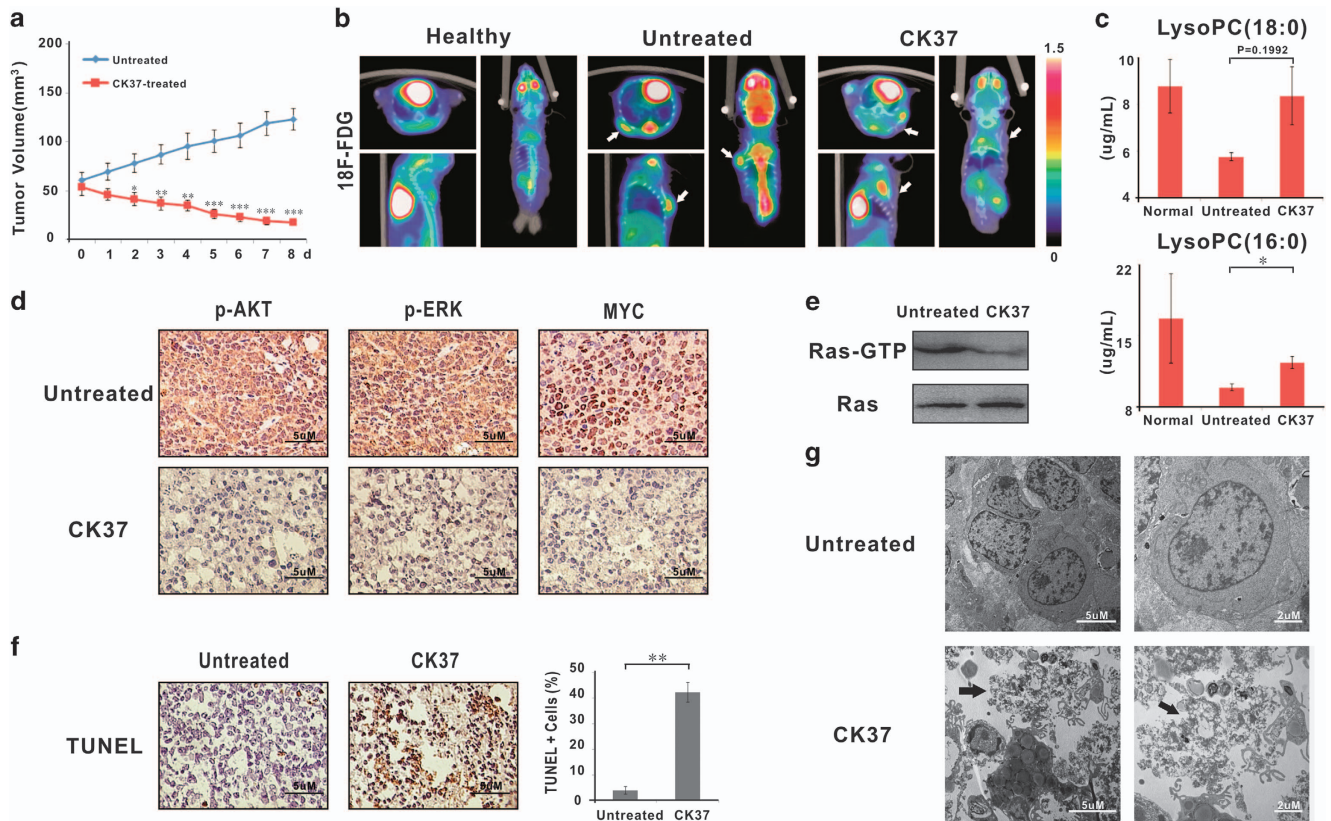


Figure 6. *In vivo* activity of CK37 on murine xenograft T-lymphoma model. **(a)** In the CK37 group, tumors grew more slowly than the untreated group. **(b)** Micro-PET/CT showed decreased standardized uptake value (SUV) intensity after CK37 treatment. **(c)** CK37 restored serum levels of choline metabolites LysoPC (18:0) and LysoPC (16:0). **(d and e)** CK37 inhibited protein levels of p-AKT, p-ERK and MYC **(d)**, as well as the activity of Ras-GTP **(e)**. **(f)** TUNEL assay showed significantly increased apoptotic cells in the CK37 group. ****P** < 0.01 compared with the untreated group. **(g)** CK37-treated tumors presented typical necroptosis morphology under transmission electron microscopy. Data in **(a)**, **(c)** and **(f)** were represented as mean \pm s.e.m.

tumors were frequently accompanied by the presence of typical necroptosis, as revealed by transmission electron microscopy (Figure 6g).

DISCUSSION

Cancer cells are characterized by their metabolic readouts. As for non-Hodgkin's lymphoma, previous research only reported on urine metabolites, using matrix-assisted laser desorption/ionization MS of low-mass range, resulting in the alteration of purine metabolism.¹⁷ In this first time serum metabolomic study on TCL, distinct metabolomic profile was identified by high-throughput UPLC-QTOFMS, providing direct evidence of aberrant choline metabolism in this disease. This is in accordance with the data obtained by less sensitive metabolomics study (proton nuclear magnetic resonance and liquid chromatography MS) from other hematological malignancies such as acute myeloid leukemia, chronic lymphocytic leukemia and multiple myeloma, in which abnormal expression of choline and its phosphorylated derivatives were detected.^{18,19} Importantly, dysregulation of choline metabolism was present in all histological types of TCL studied, consistent with acute myeloid leukemia that metabolomic status is independent of morphological classification or genetic features.²⁰ Therefore, manifested with a heterogeneous group of disease, TCL may share the similar profile of disturbed choline metabolism, and this metabolic pathway can be exploited as a source of biomarkers for TCL aggression.

Choka is a key regulator of choline metabolism. As an initial enzyme, Choka overexpression resulted in significantly increased tumor cell uptake of the affected metabolites such as choline, LysoPC (18:0), LysoPC (16:0) and AA, activation of the corresponding choline metabolic pathway and thereby decreased serum level of choline and other metabolites observed in TCL patients. Recent studies have suggested that Choka is closely related to tumor progression in solid tumors such as breast, ovarian and bladder cancer.^{21–23} Here, we demonstrated that Choka was upregulated and contributed to aberrant choline metabolism in TCL. Importantly, specific inhibition of Choka in T-lymphoma cells not only restored choline metabolites but also retarded tumor cell growth and enhanced tumor cell sensitivity to chemotherapeutic and biotherapeutic agents. Therefore, responsible for dysregulation of choline metabolism, Choka may also have a pivotal role in tumor proliferation and progression in TCL.

A reciprocal interaction between metabolic enzymes and oncogenic signaling pathways linked these enzymes to tumor progression.²⁴ As a mechanism of action, Choka is able to stimulate constitutive elevation of phospholipid-derived second messengers and interacted with cellular signaling pathways.^{7,25} For example, Choka activity is responsible for the downstream production of diacylglycerol, phosphatidic acid and lysophosphatidic acid, promoters of several Ras signaling pathways.^{26,27} In solid tumors, molecular knockdown of Choka leads to the simultaneous attenuation of AKT and ERK cascades and was associated with the inhibition of tumor cell proliferation.²⁸ Our observation confirmed that Choka acted on T-lymphoma cells

through Ras-AKT/ERK-MYC axis, reinforcing the proposed role of Choka as an oncogene in TCL, with its overexpression contributing, through a positive feedback loop, to activate oncogenic signaling pathways.

Specific inhibitors of Choka promote apoptotic cell death in solid tumors and leukemic T cells, whereas the viability of normal primary cells is not affected, indicating the therapeutic potential of targeting Choka in cancer treatment.²⁹ Indeed, a Choka inhibitor TCD-717 is currently under phase I dose escalation trial in advanced solid tumors.³⁰ Both *in vitro* and *in vivo*, our study showed that depletion of Choka generated with antitumoral activity of TCL through inducing tumor cell apoptosis in a Ras-AKT/ERK-dependent manner. Combination therapies targeting Ras-induced activation of AKT and ERK signaling have proven more effective than single pathway disruption in cancer treatment.³¹ Given that selective inhibition of Choka targeted simultaneously the two pathways, we expected that therapeutic targeting of Choka may have promising activity against TCL, as well as a broad range of hematological malignancies propagated by a diverse interruption of Ras signaling pathway.

Apart from apoptosis, we also found necroptosis in T-lymphoma cells, possibly mediated by CK37-induced TNF- α secretion. Considering that tumor cells often develop resistance to chemotherapy through acquiring antiapoptotic behavior, necroptotic susceptibility is still a weak point of cancer.³² Recent study showed that AKT inhibitor perifosine and ERK inhibitor sorafenib induce tumor cell necrosis in Hodgkin's lymphoma xenograft.³³ Choka, cotargeting AKT and ERK, also inhibited tumor growth through necroptosis, suggestive a novel molecular mechanism of Choka on TCL. Moreover, Choka inhibitors displayed a synergistic antiproliferative effect in combination with the chemotherapeutic agent.³⁰ In our study, instead of first-line chemotherapeutic agents such as doxorubicin and cyclophosphamide, CK37 synergistically interacted with second-line agents such as cisplatin and gemcitabine, as well as biotherapeutic agent histone deacetylase inhibitor valproic acid, providing useful information on the clinical efficacy of the Choka inhibitor combined with other therapeutic agents in treating TCL.

Collectively, altered choline metabolism occurred in TCL. Choline-related enzyme Choka was essential for tumor progression through the activation of downstream oncogenic Ras-AKT/ERK signaling pathways, providing a potential therapeutic target in treating TCL and other Ras-initiated hematological malignancies.

CONFLICT OF INTEREST

The authors declare no conflict of interest.

ACKNOWLEDGEMENTS

This work was supported, in part, by the National Natural Science Foundation of China (81325003, 81172254 and 81101793), the Shanghai Commission of Science and Technology (11JC1407300) and the Program of Shanghai Subject Chief Scientists (13XD1402700).

REFERENCES

- 1 Lin HN, Liu CY, Pai JT, Chang FP, Yang CF, Yu YB et al. How to predict the outcome in mature T and NK cell lymphoma by currently used prognostic models? *Blood Cancer J* 2012; **2**: e93.
- 2 Vose J, Armitage J, Weisenburger D. International peripheral T-cell and natural killer/T-cell lymphoma study: pathology findings and clinical outcomes. *J Clin Oncol* 2008; **26**: 4124–4130.
- 3 Zhao WL. Targeted therapy in T-cell malignancies: dysregulation of the cellular signaling pathways. *Leukemia* 2010; **24**: 13–21.
- 4 Valdez BC, Zander AR, Song G, Murray D, Nieto Y, Li Y et al. Synergistic cytotoxicity of gemcitabine, clofarabine and edelfosine in lymphoma cell lines. *Blood Cancer J* 2014; **4**: e171.

- 5 Hanahan D, Weinberg RA. Hallmarks of cancer: the next generation. *Cell* 2011; **144**: 646–674.
- 6 Ridgway ND. The role of phosphatidylcholine and choline metabolites to cell proliferation and survival. *Crit Rev Biochem Mol Biol* 2013; **48**: 20–38.
- 7 Glunde K, Bhujwala ZM, Ronen SM. Choline metabolism in malignant transformation. *Nat Rev Cancer* 2011; **11**: 835–848.
- 8 Ramirez de Molina A, Sarmentero-Estrada J, Belda-Iniesta C, Taron M, Ramirez de Molina V, Cejas P et al. Expression of choline kinase alpha to predict outcome in patients with early-stage non-small-cell lung cancer: a retrospective study. *Lancet Oncol* 2007; **8**: 889–897.
- 9 Ramirez de Molina A, Gutierrez R, Ramos MA, Silva JM, Silva J, Bonilla F et al. Increased choline kinase activity in human breast carcinomas: clinical evidence for a potential novel antitumor strategy. *Oncogene* 2002; **21**: 4317–4322.
- 10 Piccaluga PP, Fuligni F, De Leo A, Bertuzzi C, Rossi M, Bacci F et al. Molecular profiling improves classification and prognostication of nodal peripheral T-cell lymphomas: results of a phase III diagnostic accuracy study. *J Clin Oncol* 2014; **31**: 3019–3025.
- 11 Zhang H, Wang Y, Gu X, Zhou J, Yan C. Metabolomic profiling of human plasma in pancreatic cancer using pressurized capillary electrochromatography. *Electrophoresis* 2010; **32**: 340–347.
- 12 Tran MQ, Nygren Y, Lundin C, Naredi P, Bjorn E. Evaluation of cell lysis methods for platinum metallomic studies of human malignant cells. *Anal Biochem* 2009; **396**: 76–82.
- 13 Yan ZX, Wu LL, Xue K, Zhang QL, Guo Y, Romero M et al. MicroRNA187 overexpression is related to tumor progression and determines sensitivity to bortezomib in peripheral T-cell lymphoma. *Leukemia* 2014; **28**: 880–887.
- 14 Oki T, Kitaura J, Watanabe-Okochi N, Nishimura K, Maehara A, Uchida T et al. Aberrant expression of RasGRP1 cooperates with gain-of-function NOTCH1 mutations in T-cell leukemogenesis. *Leukemia* 2012; **26**: 1038–1045.
- 15 Fulda S. Alternative cell death pathways and cell metabolism. *Int J Cell Biol* 2013; **2013**: 463637.
- 16 Cai Z, Jitkaew S, Zhao J, Chiang HC, Choksi S, Liu J et al. Plasma membrane translocation of trimerized MLKL protein is required for TNF-induced necroptosis. *Nat Cell Biol* 2013; **16**: 55–65.
- 17 Yoo BC, Kong SY, Jang SG, Kim KH, Ahn SA, Park WS et al. Identification of hypoxanthine as a urine marker for non-Hodgkin lymphoma by low-mass-ion profiling. *BMC Cancer* 2010; **10**: 55.
- 18 Piszcz J, Lemancewicz D, Dudzik D, Ciborowski M. Differences and similarities between LC-MS derived serum fingerprints of patients with B-cell malignancies. *Electrophoresis* 2013; **34**: 2857–2864.
- 19 Wang Y, Zhang L, Chen WL, Wang JH, Li N, Li JM et al. Rapid diagnosis and prognosis of *de novo* acute myeloid leukemia by serum metabolomic analysis. *J Proteome Res* 2013; **12**: 4393–4401.
- 20 Wang JH, Chen WL, Li JM, Wu SF, Chen TL, Zhu YM et al. Prognostic significance of 2-hydroxyglutarate levels in acute myeloid leukemia in China. *Proc Natl Acad Sci USA* 2013; **110**: 17017–17022.
- 21 Gadiya M, Mori N, Cao MD, Mironchik Y, Kakkad S, Gribbestad IS et al. Phospholipase D1 and choline kinase-alpha are interactive targets in breast cancer. *Cancer Biol Ther* 2014; **15**: 593–601.
- 22 Granata A, Nicoletti R, Tinaglia V, De Cecco L, Pisanu ME, Ricci A et al. Choline kinase-alpha by regulating cell aggressiveness and drug sensitivity is a potential druggable target for ovarian cancer. *Br J Cancer* 2014; **110**: 330–340.
- 23 Hernando E, Sarmentero-Estrada J, Koppie T, Belda-Iniesta C, Ramirez de Molina V, Cejas P et al. A critical role for choline kinase-alpha in the aggressiveness of bladder carcinomas. *Oncogene* 2009; **28**: 2425–2435.
- 24 Benjamin DI, Cravatt BF, Nomura DK. Global profiling strategies for mapping dysregulated metabolic pathways in cancer. *Cell Metab* 2012; **16**: 565–577.
- 25 Marchan R, Lesjak MS, Stewart JD, Winter R, Seeliger J, Hengstler JG. Choline-releasing glycerophosphodiesterase ED3 links the tumor metabolome to signaling network activities. *Cell Cycle* 2012; **11**: 4499–4506.
- 26 Riese MJ, Wang LC, Moon EK, Joshi RP, Ranganathan A, June CH et al. Enhanced effector responses in activated CD8+ T cells deficient in diacylglycerol kinases. *Cancer Res* 2013; **73**: 3566–3577.
- 27 Stewart JD, Marchan R, Lesjak MS, Lambert J, Hergenroeder R, Ellis JK et al. Choline-releasing glycerophosphodiesterase ED3 drives tumor cell migration and metastasis. *Proc Natl Acad Sci USA* 2012; **109**: 8155–8160.
- 28 Clem BF, Clem AL, Yalcin A, Goswami U, Arumugam S, Telang S et al. A novel small molecule antagonist of choline kinase-alpha that simultaneously suppresses MAPK and PI3K/AKT signaling. *Oncogene* 2011; **30**: 3370–3380.

- 29 Banez-Coronel M, Ramirez de Molina A, Rodriguez-Gonzalez A, Sarmentero J, Ramos MA, Garcia-Cabezas MA *et al*. Choline kinase alpha depletion selectively kills tumoral cells. *Curr Cancer Drug Targets* 2008; **8**: 709–719.
- 30 de la Cueva A, Ramirez de Molina A, Alvarez-Ayerza N, Ramos MA, Cebrian A, Del Pulgar TG *et al*. Combined 5-FU and ChoKalpha inhibitors as a new alternative therapy of colorectal cancer: evidence in human tumor-derived cell lines and mouse xenografts. *PLoS One* 2013; **8**: e64961.
- 31 Watson AL, Anderson LK, Greeley AD, Keng VW, Rahrmann EP, Halfond AL *et al*. Co-targeting the MAPK and PI3K/AKT/mTOR pathways in two genetically engineered mouse models of schwann cell tumors reduces tumor grade and multiplicity. *Oncotarget* 2014; **5**: 1502–1514.
- 32 Declercq W, Vanden Berghe T, Vandenabeele P. RIP kinases at the crossroads of cell death and survival. *Cell* 2009; **138**: 229–232.
- 33 Locatelli SL, Giacomini A, Guidetti A, Cleris L, Mortarini R, Anichini A *et al*. Perifosine and sorafenib combination induces mitochondrial cell death and antitumor effects in NOD/SCID mice with Hodgkin lymphoma cell line xenografts. *Leukemia* 2013; **27**: 1677–1687.



This work is licensed under a Creative Commons Attribution-NonCommercial-NoDerivs 4.0 International License. The images or other third party material in this article are included in the article's Creative Commons license, unless indicated otherwise in the credit line; if the material is not included under the Creative Commons license, users will need to obtain permission from the license holder to reproduce the material. To view a copy of this license, visit <http://creativecommons.org/licenses/by-nc-nd/4.0/>

Supplementary Information accompanies this paper on Blood Cancer Journal website (<http://www.nature.com/bcj>)